Hassen BELILA[1], Nasserdine BOUDJERDA[2], Imen BAHRI[3], Ahsene BOUBAKIR[4]

LENT Laboratory,University of of Oum El Bouaghi, Algeria (1), LER Laboratory, University of Jijel, Algeria (2)
University of Paris-Saclay, France (3), LAJ Laboratory, University of Jijel, Algeria (4)
ORCID: 0000-0003-0220-0236

Robust Hybrid Control Strategy PI-Sliding Mode Control of a STATCOM in the Presence of a Decentralized PV Source

Abstract. Nowadays, the flexible alternating current transmission systems (FACTS) have emerged and began to play a key role in improving the quality of the grid power. The aim of this work is to design a robust control strategy for the voltage and the flow of reactive power using one of the most popular FACTS devices, namely the STATCOM (static compensator). The proposed strategy consists of a hybrid control (PI control - sliding mode control). This strategy proved its effectiveness in terms of response time and harmonic distortion rate. Furthermore, we investigated the impact of the insertion of a photovoltaic source in the electrical network on the STATCOM operation. Simulation results show that this decentralized source has relieved the grid by its contribution in active power with practically no influence on the performance of the STATCOM, which remains unaffected.

*Streszczenie. Obecnie pojawiły się elastyczne systemy przesyłu prądu przemiennego (FACTS), które zaczęły odgrywać kluczową rolę w poprawie jakości energii sieciowej. Celem pracy jest zaprojektowanie solidnej strategii sterowania napięciem i przepływem mocy biernej za pomocą jednego z najpopularniejszych urządzeń FACTS, czyli STATCOM (kompensator statyczny). Proponowana strategia składa się ze sterowania hybrydowego (regulacja PI – sterowanie ślizgowe). Strategia ta dowiodła swojej skuteczności pod względem czasu odpowiedzi i współczynnika zniekształceń harmonicznych. Ponadto zbadaliśmy wpływ wprowadzenia źródła fotowoltaicznego do sieci elektrycznej na działanie STATCOM. Wyniki symulacji pokazują, że to zdecentralizowane źródło odciążyło sieć dzięki swojemu udziałowi w mocy czynnej, praktycznie bez wpływu na wydajność STATCOM, na co nie ma to wpływu. (**Odporna strategia sterowania hybrydowego Sterowanie trybem przesuwnym PI STATCOM w obecności zdecentralizowanego źródła PV**)*

Keywords: STATCOM, PV source, sliding mode control, reactive power compensation, harmonics
Słowa kluczowe: STATCOM, sterowaniem zdecentralizowane źródło

Introduction

Grid-connected decentralized sources have evolved greatly in recent years. Electricity system deregulation and competition have been implemented in many regions of the world to lower customer energy costs, improve supply security, and promote efficiency [1]. The use of renewable resources stimulates the incorporation of more renewable energy generators into electrical systems to reduce greenhouse gas emissions [2].

The rapid development of power electronics has resulted in a significant impact on improving power grid operation by introducing control devices based on advanced power electronic components (GTO, IGBT), known as FACTS (Flexible Alternative Current Transmission Systems) [3]. These converters can be classified based on their network connection as shunt, series, or hybrid compensators, such as STATCOM (STATic COMpensator), SSSC (Static Synchronous Series Compensator), and UPFC (Unified Power Flow Controller), respectively.

The STATCOM is one of the most widely used devices for reactive energy compensation and voltage regulation at the common coupling point (CCP). It generates a three-phase AC voltage synchronized with the grid one from a DC voltage source. No active power is involved; only reactive power is exchanged between the STATCOM and the grid, allowing both the correction of power factor and compensation for voltage drops and overvoltage, hence improving the power quality [3]–[5].

Many extensive studies over the past few years have revealed that the success of STATCOM is heavily dependent on the accuracy and robustness of the control approach used [6], [7]. Traditional, PI controllers are simple to implement, however they are heavily affected by parameter variations and may suffer from stability issues. In the reference [8] the authors present an adaptive PI control of a STATCOM in order to maintain control performance under changing system conditions. In [9] and [10], fuzzy logic controls are suggested for D-STATCOMs (D-STATCOM: STATCOM coupled to a distribution network) to improve voltage stability, dampen power oscillations, and improve transient stability compared to conventional PI control. The authors of reference [11] proposed a D-STATCOM to adjust the output voltage of a hybrid power plant (wind-diesel unit), and a sliding mode control was used. The authors of reference [12] attempt to improve the performance of a D-STATCOM by selecting an appropriate DC reference, this method reduces switching losses and current harmonics of the D-STATCOM without degrading its dynamic. The authors of reference [13] used a hybrid approach (SMC-PI) on a D-STATCOM to increase both static and dynamic performance over the usual PI configuration.

In this paper, we investigate the compensation of the power grid using a STATCOM in the presence of a decentralized PV source. As the STATCOM's control methodology is critical for good static and dynamic performance, we propose a hybrid strategy (PI control-sliding mode control). Also, the PV source is connected to the grid using a sliding mode control strategy. In section two and three, the grid connected STATCOM and the grid connected PV source are modeled respectively. The sliding mode control proposed for both the STATCOM and the PV source is developed in section four. Section five is devoted to the simulation results and analysis. Finally, we give the conclusions.

Modeling of the grid connected STATCOM

The STATCOM is represented by the equivalent diagram of (Fig.1).

Only the bus bar of the common coupling point (CCP) is considered and the DC source is assumed to be constant (Fig.1.a). The equivalent circuit of (Fig.1.b) is an AC voltage source v_{sh} connected to the network by the inductor (L_{sh}, R_{sh}) of the coupling transformer [14]. The reactive power exchanged between the STATCOM and the grid is adjusted by action on the amplitude of the STATCOM voltage v_{sh}. This reactive energy is either injected into the network or extracted from the network, allowing the bus bar voltage v_r to be regulated at a desired value [15].

a. Block diagram   b. Equivalent circuit
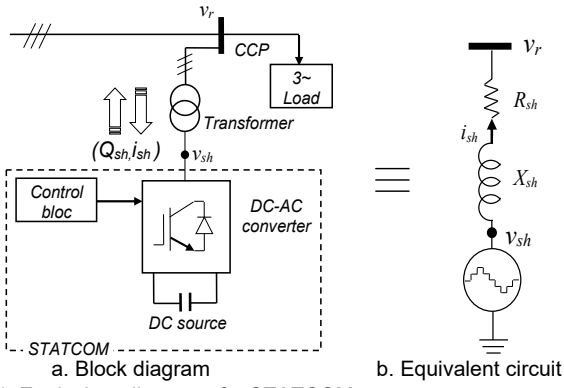
Fig.1. Equivalent diagram of a STATCOM

In the per unit system, the application of Kirchhoff's laws on the equivalent circuit of Fig.1.b gives:

$$(1) \quad \begin{cases} v_{sha} - v_{ra} = R_{sh}i_{sha} + L_{sh}\dfrac{di_{sha}}{dt} \\ v_{shb} - v_{rb} = R_{sh}i_{shb} + L_{sh}\dfrac{di_{shb}}{dt} \\ v_{shc} - v_{rc} = R_{sh}i_{shc} + L_{sh}\dfrac{di_{shc}}{dt} \end{cases}$$

(v_{ra}, v_{rb}, v_{rc}): Three phase voltages at the CCP.

(v_{sha}, v_{shb}, v_{shc}): Three phase STATCOM output voltages.

(i_{sha}, i_{shb}, i_{shc}): Three phase currents of the STATCOM.

The Park transformation allows the transition from a balanced three phase system (*a,b,c*) to a two axes rotating (*d, q*) frame [15]:

$$(2) \quad \begin{bmatrix} x_d \\ x_q \end{bmatrix} = [P(\theta)] \begin{bmatrix} x_a \\ x_b \\ x \end{bmatrix}$$

Where (x_a, x_b, x_c) are phase components of the three phase system (voltage, current …), (x_d, x_q) are Park components, θ is the angle between the phase axis *a* and the rotating axis *d*, $[P(\theta)]$ is the transformation matrix.

Considering $\theta = 2\pi f t$ (*f*: frequency of the grid currents), the park transform of equation (1) gives [16]:

$$(3) \quad \begin{cases} v_{shd} - v_{rd} = R_{sh}i_{shd} + L_{sh}\dfrac{di_{shd}}{dt} - \omega L_{sh}i_{shq} \\ v_{shq} - v_{rq} = R_{sh}i_{shq} + L_{sh}\dfrac{di_{shq}}{dt} + \omega L_{sh}i_{shd} \end{cases}$$

Then, the state equation of the STATCOM is written as follows:

$$(4) \quad \begin{cases} \dfrac{d}{dt}i_{shd} = -\dfrac{R_{sh}}{L_{sh}}i_{shd} + \omega.i_{shq} - \dfrac{1}{L_{sh}}v_{rd} + \dfrac{1}{L_{sh}}u_1 \\ \dfrac{d}{dt}i_{shq} = -\dfrac{R_{sh}}{L_{sh}}i_{shq} - \omega.i_{shd} - \dfrac{1}{L_{sh}}v_{rq} + \dfrac{1}{L_{sh}}u_2 \end{cases}$$

$\begin{bmatrix} v_{shd} \\ v_{shq} \end{bmatrix} = \begin{bmatrix} u_1 \\ u_2 \end{bmatrix}$: Input vector of the system.

$\begin{bmatrix} i_{shd} \\ i_{shq} \end{bmatrix}$: State variables of the system.

Grid connected PV source using three-phase inverter
Fig.2 shows the proposed direct three-phase grid-connected PV system, including a solar array, a capacitive DC link, and a three-phase inverter with an inductive filter (*R*, *L*). To obtain the needed dc voltage (v_{dc}) and power rating,

the PV modules are connected in a series–parallel configuration. Note that commonly two converters are used; a DC-DC converter for adjusting the MPPT and a DC-AC converter for controlling the reactive power injected into the network. In our work, only a three-phase inverter is used in the proposed simple conversion system.
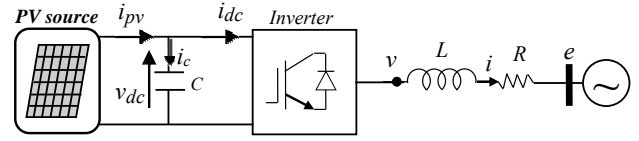
Fig.2. Direct grid connected PV source using three-phase inverter

Photovoltaic source
PV sources convert emitted solar energy into electrical energy. We use the simplified model shown in Fig.3 to derive the features and behavior of a PV cell [17].
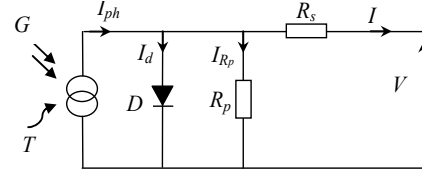
Fig.3. Circuit diagram of the PV cell model

The modeling of the solar cell is defined by the following voltage–current relationship [18]:

$$(5) \quad I = I_{ph} - I_s\left[\exp\left(\frac{q(V + R_sI)}{N_skTa}\right) - 1\right] - \frac{V + R_s.I}{R_p}$$

where: *I*: PV output current (A).; I_{ph}: Cell's photocurrent.; I_s: Saturation current (A).; *V*: PV output voltage (V).; *q*: Electron charge (1.60217×10^{-19} C).; *k*: Boltzmann constant (1.38065×10^{23} J/K); *a*: Diode ideality constant; R_s and R_P: Series and parallel resistances of cell (Ω); Ns: Number of cells in series; *T*: Temperature (K).

More details on the modeling of a PV cell can be found in [17]. In our work, we use the BP3160 module, the parameters of which are detailed in Table 1.

Table 1. Specifications of PV module BP3160, [17]

Characteristics	Values
Typical peak power	160 W
Voltage at peak power	34.5 V
Current at peak power	4.55 A
Short-circuit current (I_{sc})	4.8 A
Open circuit voltage (V_{oc})	44.2 V
Temperature coefficient of I_{sc} (k_1)	(0.065±0.015) %/K
Temperature coefficient of V_{oc} (k_2)	(160±20) mV/K
Factor of PV technology (*a*)	1.5
Series resistance (R_s)	5 mΩ

According to Fig.2, the AC-side of the inverter is governed by the following equations:

$$(6) \quad \begin{cases} v_a = R\,i_a + L\dfrac{di_a}{dt} + e_a \\ v_b = R\,i_b + L\dfrac{di_b}{dt} + e_b \\ v_c = R\,i_c + L\dfrac{di_c}{dt} + e_c \end{cases}$$

In the rotating (*d, q*) frame, equation (6) becomes:

$$(7) \quad \begin{bmatrix} v_d \\ v_q \end{bmatrix} = R\begin{bmatrix} i_d \\ i_q \end{bmatrix} + L\frac{d}{dt}\begin{bmatrix} i_d \\ i_q \end{bmatrix} - L\omega\begin{bmatrix} i_q \\ -i_d \end{bmatrix} + \begin{bmatrix} e_d \\ e_q \end{bmatrix}$$

where (e_d, e_q, i_d, i_q, v_d, v_q) are the components of grid voltage, grid current and inverter output voltage respectively. Neglecting the power losses in the inverter switches, the power balance relationship between the DC side and the AC side is given by:

(8) $$e_d.i_d + e_q.i_q = v_{dc}.i_{dc}$$

Where, v_{dc} and i_{dc} are the input voltage and current of the inverter, respectively. Applying Kirchoff law on the DC side of the inverter (Fig.2) yields to the following equation:

(9) $$C.\frac{dv_{dc}}{dt} = i_{pv} - i_{dc} = i_{pv} - \frac{e_d.i_d + e_q.i_q}{v_{dc}}$$

Where, i_{pv} is the output current of the PV array
Then, equations (7) and (9) are grouped as follows:

(10) $$\dot{x} = \begin{bmatrix} -\dfrac{R}{L}i_d + \omega.i_q - \dfrac{e_d}{L} \\ -\dfrac{R}{L}i_q - \omega.i_d - \dfrac{e_q}{L} \\ \dfrac{i_{pv}}{C} - \dfrac{e_d.i_d + e_q.i_q}{C.v_{dc}} \end{bmatrix} + \begin{bmatrix} \dfrac{1}{L} & 0 \\ 0 & \dfrac{1}{L} \\ 0 & 0 \end{bmatrix}.u$$

where: $u = (u_3, u_4)^T = (v_d, v_q)^T$ is the input vector; $x = (x_1, x_2, x_3)^T = (i_d, i_q, v_{dc})^T$ is the state vector; Equation (10) can be written in the following form:

(11) $$\dot{x} = f(x) + g(x).u$$

Where, $f(x)$ and $g(x)$ are defined by:

$$f(x) = \begin{bmatrix} f_1(x) \\ f_2(x) \\ f_3(x) \end{bmatrix} = \begin{bmatrix} -\dfrac{R}{L} \cdot x_1 + \omega \cdot x_2 - \dfrac{e_d}{L} \\ -\dfrac{R}{L} \cdot x_2 - \omega \cdot x_1 - \dfrac{e_q}{L} \\ \dfrac{i_{pv}}{C} - \dfrac{e_d \cdot x_1 + e_q \cdot x_2}{C \cdot x_3} \end{bmatrix}$$

$$g(x) = \begin{bmatrix} \dfrac{1}{L} & 0 \\ 0 & \dfrac{1}{L} \\ 0 & 0 \end{bmatrix}$$

Sliding mode control of STATCOM and PV Application to the STATCOM

According to equation (3), the relative degrees of outputs $x_1 = i_{shd}$ and $x_2 = i_{shq}$ are unitary, i.e. $r_1 = r_2 = 1$. To improve the steady-state tracking performance, we have adopted the following integral-type sliding surfaces [19]:

(12) $$S_1 = \left(\frac{d}{dt} + \lambda_1\right)\int_0^t e_1$$

(13) $$S_2 = \left(\frac{d}{dt} + \lambda_2\right)\int_0^t e_2$$

Where: (14) $e_1 = i^*_{shd} - i_{shd}$,

(15) $$e_2 = i^*_{shq} - i_{shq}$$

By inserting equations (14) and (15) into (12) and (13), respectively, we obtain the following derivatives:

(16) $$\dot{S}_1 = i^*_{shq} - i_{shq} + \lambda_1.e_1$$

(17) $$\dot{S}_2 = i^*_{shq} - i_{shq} + \lambda_2.e_2$$

By inserting equations (3) into (16) and (17), we get

(18) $$\dot{S}_1 = i^*_{shd} + \frac{R_{sh}}{L_{sh}}i_{shd} - \omega.i_{shq} + \frac{1}{L_{sh}}v_{rd} - \frac{1}{L_{sh}}u_1 + \lambda_1.e_1$$

(19) $$\dot{S}_2 = i^*_{shq} + \frac{R_{sh}}{L_{sh}}i_{shq} + \omega.i_{shd} + \frac{1}{L_{sh}}v_{rq} - \frac{1}{L_{sh}}u_2 + \lambda_2.e_2$$

And, in order to check Lyapunov stability criterion ($S_i.\dot{S}_i < 0$), we must have:

(20) $$\dot{S}_1 = -\alpha_1 S_1 - \beta_1 \, sign(S_1)$$

(21) $$\dot{S}_2 = -\alpha_2 S_2 - \beta_2 sign(S_2)$$

Where α_1, α_2, β_1 and β_2 are design parameters, allowing the designer to improve closed loop response time and robustness against the effect of uncertainties and exogenous inputs. The greater the α_1 and α_2 values, the faster the attraction time to the sliding surface, while small values of β_1 and β_2 reduce oscillations.

By equaling equations (18) with (20) and (19) with (21), we get:

(22) $$i^*_{shd} + \frac{R_{sh}}{L_{sh}}i_{shd} - \omega.i_{shq} + \frac{1}{L_{sh}}v_{rd} - \frac{1}{L_{sh}}u_1 + \lambda_1.e_1$$
$$= -\alpha_1 S_1 - \beta_1 \, sign(S_1)$$

(23) $$i^*_{shq} + \frac{R_{sh}}{L_{sh}}i_{shq} + \omega.i_{shd} + \frac{1}{L_{sh}}v_{rq} - \frac{1}{L_{sh}}u_2 + \lambda_2.e_2$$
$$= -\alpha_2 S_2 - \beta_2 sign(S_2)$$

This allows us to find u_1 and u_2 command expressions:

(24) $$u_1 = L_{sh}i^*_{shd} + R_{sh}i_{shd} - L_{sh}\omega.i_{shq} + v_{rd} + L_{sh}\lambda_1 e_1$$
$$+ \alpha_1 L_{sh}S_1 + \beta_1 L_{sh}\, sign(S_1)$$

(25) $$u_2 = L_{sh}i^*_{shq} + R_{sh}i_{shq} + L_{sh}\omega.i_{shd} + v_{rq} + L_{sh}\lambda_2 e_2$$
$$+ \alpha_2 L_{sh}S_2 + \beta_2 L_{sh}\, sign(S_2)$$

Taking into consideration:

(26) $$u_1 = u_{eq1} + u_{c1}$$

(27) $$u_2 = u_{eq2} + u_{c2}$$

The following order and correction terms are obtained:
- Equivalent order terms u_{eq1} and u_{eq2} :

(28) $$u_{eq1} = L_{sh}i^*_{shd} + R_{sh}i_{shd} - L_{sh}\omega.i_{shq} + v_{rd} + L_{sh}\lambda_1 e_1$$

(29) $$u_{eq2} = L_{sh}i^*_{shq} + R_{sh}i_{shq} + L_{sh}\omega.i_{shd} + v_{rq} + L_{sh}\lambda_2 e_2$$

- Correction terms u_{c1} and u_{c2} :

(30) $$u_{c1} = \alpha_1 L_{sh}S_1 + \beta_1 L_{sh}\, sign(S_1)$$

(31) $$u_{c2} = \alpha_2 L_{sh}S_2 + \beta_2 L_{sh}\, sign(S_2)$$

Finally, the control of the two internal variables (i_{shd} and i_{shq}) is achieved by a SMC block as shown in (Fig.4).

The DC bus voltage control loop keeps v_{dc} constant by controlling the active power transit between the PCC and the continuous bus; this voltage is frequently controlled by a PI type corrector as in (Fig.4), [20].
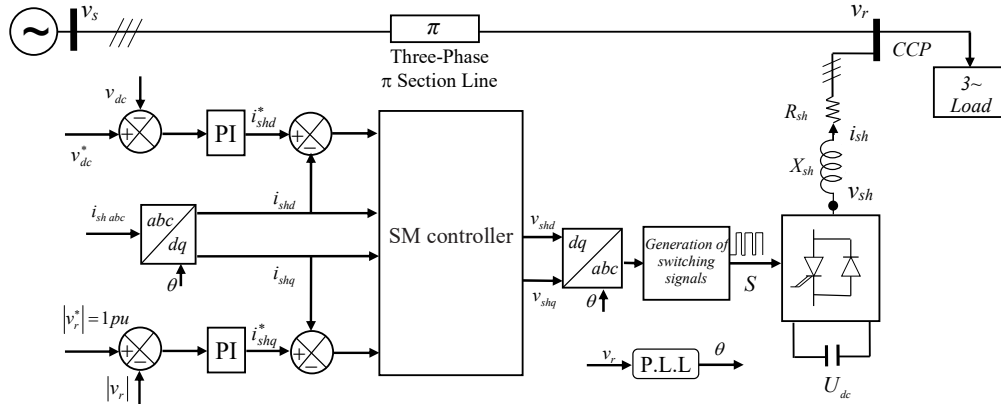
Fig.4. Block diagram of SM control strategy for STATCOM [19]

The voltage v_r at the common coupling point 'CCP' is regulated by controlling the exchange of reactive power between the STATCOM and the power grid. For this purpose, a PI controller generates a reference signal i^*_{sha} for the reactive current component of the STATCOM, (Fig.4).

Application to the PV source

The grid connection of the PV source is controlled using the sliding mode as in Fig.5.

As we have to control two variables (i_q and v_{dc}), two sliding surfaces are required, as follows:

$$(32) \qquad S_3 = e_3$$

$$(33) \qquad S_4 = \dot{e}_4 + \lambda e_4$$

where: $e_3 = i^*_q - i_q$ and $e_4 = v^*_{dc} - v_{dc}$

The time derivatives of the filtered errors given by (32) and (33), can be rewritten as follows:

$$(34) \qquad \dot{S}_3 = \dot{i}^*_q - \dot{i}_q$$

$$(35) \qquad \dot{S}_4 = \left(\ddot{v}^*_{dc} - \ddot{v}_{dc} \right) + \lambda \dot{e}_4$$
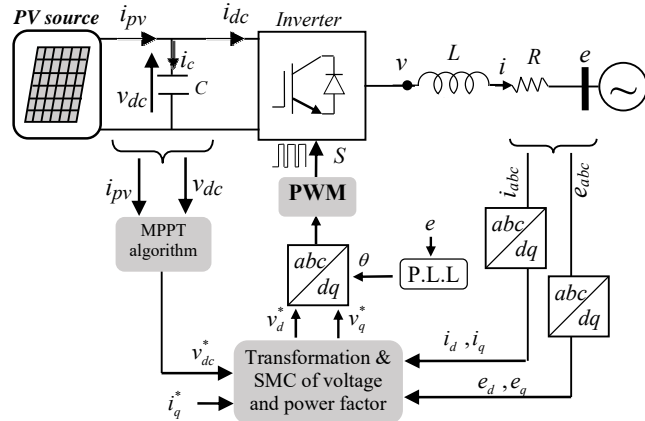
Fig.5. Block diagram of SM control strategy for PV

Then, by combining equation (10) with (32) to (35), we obtain:

$$(36) \qquad \underbrace{\begin{pmatrix} \dot{S}_3 \\ \dot{S}_4 \end{pmatrix}}_{\dot{S}} = \left[\begin{pmatrix} \dot{i}^*_q \\ \ddot{v}^*_{dc} + \lambda \dot{e}_2 \end{pmatrix} - A(x) \right] - B(x) \underbrace{\begin{pmatrix} u_3 \\ u_4 \end{pmatrix}}_{u}$$

where:

$$(37) \qquad A(x) = \begin{pmatrix} \dfrac{i_{pv}}{C} - \dfrac{e_d \cdot f_1 + e_q \cdot f_2}{C x_3} + \dfrac{e_d \cdot x_1 + e_q \cdot x_2}{C x_3^2} f_3 \\ f_2 \end{pmatrix}$$

$$(38) \qquad B(x) = \begin{pmatrix} 0 & \dfrac{1}{L} \\ \dfrac{-e_d}{LC x_3} & \dfrac{-eq}{LC x_3} \end{pmatrix}$$

Lyapunov's stability is verified by the following equation:

$$(39) \qquad \dot{S} = -\begin{pmatrix} k_{11} & 0 \\ 0 & k_{12} \end{pmatrix} S + \begin{pmatrix} k_{21} & 0 \\ 0 & k_{22} \end{pmatrix} sign(S)$$

Where, k_{11}, k_{12}, k_{21} and k_{22} are positive constants.
Combining equations (36) and (39) gives:

$$(40) \qquad \begin{aligned} &\begin{pmatrix} \dot{i}^*_q \\ \ddot{v}^*_{dc} + \lambda \dot{e}_2 \end{pmatrix} - A(x) - B(x).u \\ &= -\begin{pmatrix} k_{11} & 0 \\ 0 & k_{12} \end{pmatrix} S - \begin{pmatrix} k_{21} & 0 \\ 0 & k_{22} \end{pmatrix} sign(S) \end{aligned}$$

Thus, we obtain the following expression for the u command:

$$(41) \qquad \begin{aligned} u &= B(x)^{-1} \cdot \left[\begin{pmatrix} \dot{i}^*_q \\ \ddot{v}^*_{dc} + \lambda \dot{e}_2 \end{pmatrix} - A(x) \right] \\ &+ B(x)^{-1} \cdot \left(\begin{pmatrix} k_{11} & 0 \\ 0 & k_{12} \end{pmatrix} S + \begin{pmatrix} k_{21} & 0 \\ 0 & k_{22} \end{pmatrix} sign(S) \right) \end{aligned}$$

Finally, the u command is defined by the following terms:

- The equivalent order terms u_{eq3} and u_{eq4}:

$$(42) \qquad \begin{pmatrix} u_{eq3} \\ u_{eq4} \end{pmatrix} = B(x)^{-1} \left(\begin{pmatrix} \dot{i}^*_q \\ \ddot{v}^*_{dc} + \lambda \dot{e}_2 \end{pmatrix} - A(x) \right)$$

- The correction terms u_{c3} and u_{c4}:

$$(42) \qquad \begin{pmatrix} u_{c3} \\ u_{c4} \end{pmatrix} = B(x)^{-1} \left(K_1 S + K_2 sign(S) \right)$$

Where:

$$K_1 = \begin{pmatrix} k_{11} & 0 \\ 0 & k_{12} \end{pmatrix} \text{ and } K_2 = \begin{pmatrix} k_{21} & 0 \\ 0 & k_{22} \end{pmatrix} \quad \left. \begin{matrix} k_{1i} > 0 \\ k_{2i} > 0 \end{matrix} \right| i = 1,2$$

Simulations and results analysis
Simulations

Fig.6 presents a single-line diagram of the power network used to validate the operation of the proposed STATCOM and PV source.
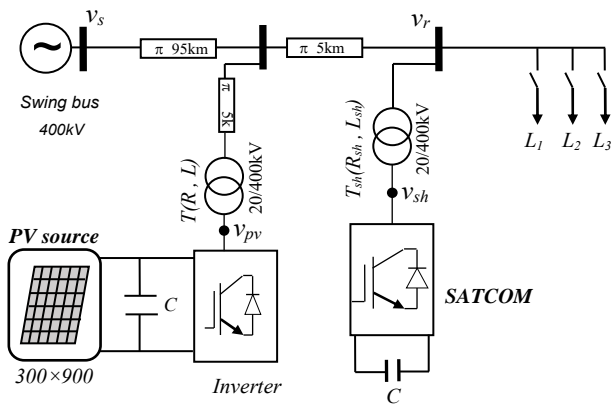
Fig.6. Single-line diagram of the studied network

The considered network is composed of a 400 kV reference generator and a transmission line modeled in π to supply three loads (L_1, L_2, and L_3) at the load bus bar " r ". The T_{sh} and T transformers reduce the voltage from 400 kV (grid voltage) to 20 kV (STATCOM and PV output voltages).

The simulations are carried out in per unit system with base values of S_B = 1000 MVA and U_B = 400 kV, while the voltage of the generator bus bar is V_S = 1.0 pu. The loads (L_1, L_2, and L_3) are connected to the busbar " r " during the three intervals shown in Table 2.

Table 2. Load variation

Time(s)	0s to 0.5s	0.5s to 1s	1s to 1.5s	1.5s to 2s
Load	L_1	$L_1 + L_2$	$L_1 + L_2 + L_3$	L_3

L_1 (inductive load): P_1 = 1.0 pu and Q_1 = 0.4 pu.
L_2 (inductive load): P_2 = 0.5 pu and Q_2 = 0.4 pu.
L_3 (capacitive load): P_3 = 0.3 pu, Q_{3C} = 0.2 pu and Q_{3L} = 0.01 pu.

Results analysis
STATCOM connection without the PV source
Fig.7 shows the voltages V_r and V_s before and after compensation.

a. Before compensation

b. After compensation
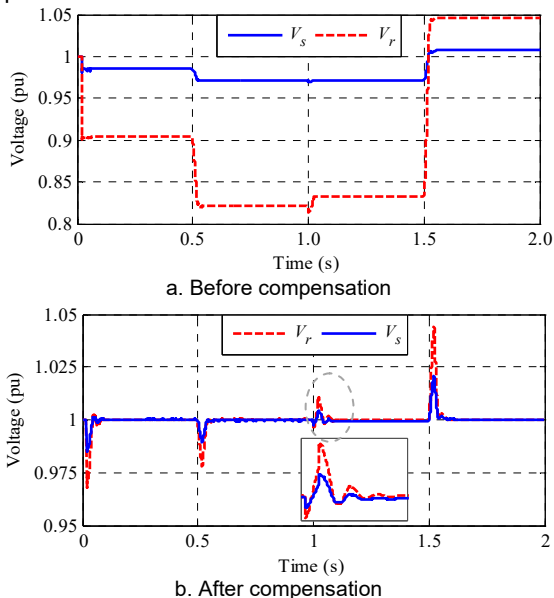
Fig.7. Source and load voltages (V_s and V_r) before and after compensation

The connection of the inductive load before compensation at t = 0.5 s (Fig.7.a), causes a voltage drop in both v_r and v_s. At time t = 1 s, the capacitive load connection L_3 reduces this voltage drop. Finally, disconnecting all

inductive loads at t = 1.5 s resulted in capacitive load flow, inducing an overvoltage both at v_r and v_s. After compensation (Fig.7.b), the voltage v_r is well regulated at its nominal value of 1.0 pu, also a favorable effect is observed on the voltage v_s, which approaches its nominal value.

In Fig.8, the exchanged reactive power between the STATCOM and the grid is shown: In inductive mode, the STATCOM injects different quantities of reactive power to raise the voltage v_r to 1.0 pu ($Q_{sh} \approx$ 0.45 pu for $0 < t < 0.5$ s, $Q_{sh} \approx$ 0.91 pu for 0.5 s $< t < 1$ s, and $Q_{sh} \approx$ 0.76 pu for 1 s $< t < 1.5$ s). In capacitive mode, the STATCOM absorbs reactive energy from the network to keep the voltage profile v_r constant, ($Q_{sh} \approx$ - 0.25 pu for 1.5 s $< t < 2$ s). Note that there is no exchange of active power.
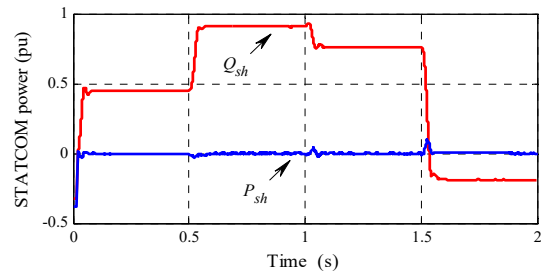
Fig.8. STATCOM Active and reactive power P_{sh} and Q_{sh}

Fig.9. shows the phase shift between the voltage and current of the source (v_{sa} and i_{sa}) before and after compensation. It appears clearly that after compensation, v_{sa} and i_{sa} are in phase; indicating that there is no transit of reactive power between the source and the load.

a. Before compensation   b. After compensation
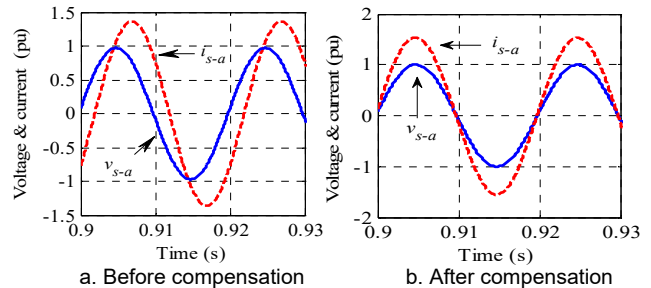
Fig.9. Phase shift between grid voltage v_s and grid current i_s before and after compensation

Overall, the hybrid (PI-SMC) control strategy is much more effective than classical PI control strategy as it gives faster dynamics with less oscillation and better grid power quality [13], [19].

Effect of the PV source on STATCOM operation
We present briefly the simulation results of the control of both the DC bus voltage v_{dc} to get the MPP and the power factor at the inverter output at a wanted value (the max value is the unity and corresponds to i_q = 0). Two perturbations are considered:

- Irradiation change from G = 1 kW/m² to 0.6 kW/m², between t = 0.6 s and t = 0.8 s.
- Temperature change from T = 25 °C to 50 °C, between t = 1.6 s and t = 1.8 s.

In Fig.10, the output voltage of the PV source is clearly shown to follow its reference identified by the MPPT-P&O algorithm and converges towards the maximum power point corresponding to (v_{dc} = 32 kV, I_{pv} = 1.3 kA, and P_{pv} = 41.6 MW) after a very short transient of about 0.15 s. The effect of atmospheric changes is also highlighted:

- The positive effect of the increase in illumination.
- The negative effect of the increase in temperature.

On the other hand, the i_q component is held at its zero-reference value (corresponding to a unit power factor).

(a) dc voltage   (b) PV Output current

(c) PV Output power   (d) i_d and i_q Grid current
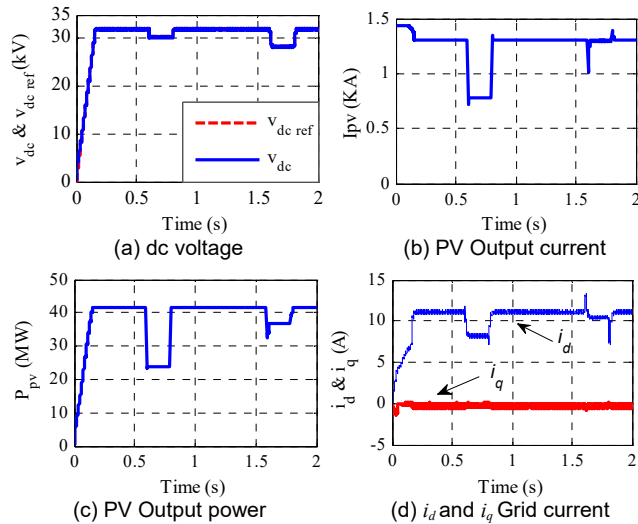
Fig.10. The PV-SMC Performances

In the following application, we consider the load voltage v_r after compensation in the presence of the photovoltaic source connected 5 km away from the load (Fig.6). Figure 11 shows that v_r is well regulated at its reference value ($v_r \approx 1.0$ pu) with and without the PV source. Thus, the PV system has practically no effect on STATCOM performance.
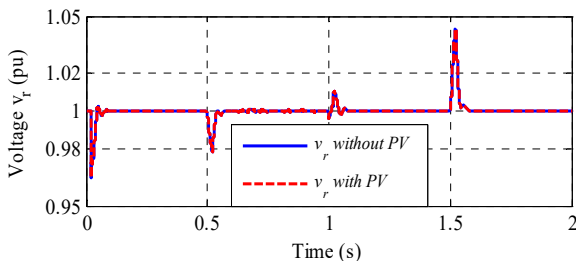
Fig.11. Voltage v_r after compensation with and without the PV source

In order to highlight the power P_{pv} generated by the PV source under ambient atmospheric conditions (T = 25°C and G = 1 kW/m^2), we show in Fig.12 the active power transit through the grid. The active power absorbed by the load (P_r) is equal to the sum of the powers injected by the two sources: the v_s source (P_s) and the PV source (P_{pv}).
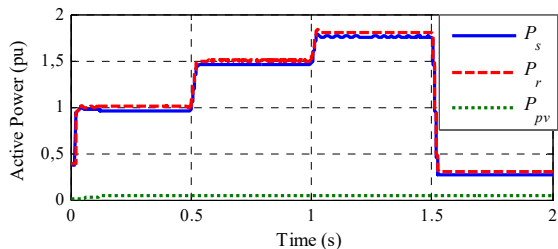
Fig.12. Active power

To see the influence of the atmospheric disturbances on the operation of the STATCOM, we compare in Fig. 13 between the shapes of the voltage v_r (with the same load profile of Fig.11) in the presence of the PV source with and without atmospheric disturbances (with the same atmospheric changes of Fig.10); the STATCOM is not affected and works regularly.
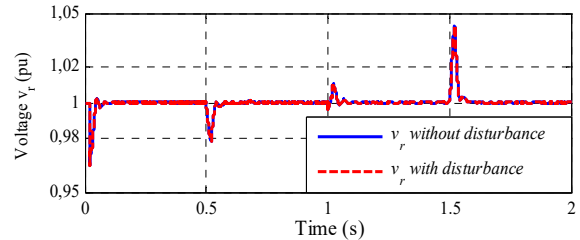
Fig.13. Voltage v_r after compensation with connected PV source with and without atmospheric disturbances

Conclusion

First, we highlighted the detrimental effect of reactive power flow on the voltage of the load bus bar. Then, the use of the STATCOM allowed adjusting for reactive power and keeping the voltage at its nominal value with a very fast dynamic and good power quality.

Secondly, we investigated the insertion effect of a decentralized source (PV source) on the operation of the STATCOM. Thanks to its active power contribution, this decentralized source has relieved the grid. Furthermore, it has practically no effect on the operation performance of the STATCOM, which keeps unaffected performance. Finally, we conclude that our control (PI-SMC) is robust with respect to the penetration of the decentralized source (PV) into the electrical network.

Authors:
Hassen Belila. University of Oum El Bouaghi, Algeria, Science and Applied Sciences Faculty, LENT Laboratory, 04000 Oum El Bouaghi, Algeria, E-mail: hassenbelila@yahoo.fr;
Nasserdine Boudjerda. University of Jijel, Algeria, Faculty of sciences and Technology, LER Laboratory, B.P 98 Ouled Aissa Jijel, Algeria, E-mail: n_boudjerda@yahoo.fr;
Imen Bahri. University of Paris-Saclay, Group of Electrical Engineering, Paris (GeePs), UMR CNRS 8507, 3 rue Joliot-Curie, Plateau de Moulon 91192 Gif-sur-Yvette CEDEX, France, E-mail: imen.bahri@centralesupelec.fr;
Ahsene Boubakir. University of Jijel, Algeria, Faculty of sciencs and Technology, LAJ Laboratory, B.P 98 Ouled Aissa Jijel, Algeria; E-mail: ah_boubakir@yahoo.fr;

REFERENCES
[1] Lai L. L., Power System Restructuring and Deregulation: Trading, Performance and Information Technology, in *JOHNWILEY &SONS, LTD Chichester*, 2001, p. 498.
[2] Widyan M. S., Hanitsch R. E., Operating point stability analysis of SMIB power system equipped with high PV penetration, *International Journal of Electrical Power and Energy Systems*, vol. 55, pp. 522–530, 2014, doi: 10.1016/j.ijepes.2013.09.031.
[3] Sen K. K., Sen M. L., Introduction to FACTS Controllers: Theory, Modeling, and Applications, in *Wiley-IEEE Press*, 2009, p. 552.
[4] Mahajan S. D., Murali M., Mali T. B., Comparative analysis of 6, 12 and 48 pulse T-STATCOM, *IEEE 7th Power India International Conference, PIICON*, 2016, doi: 10.1109/POWERI.2016.8077252.
[5] Mosaad M. I., Model reference adaptive control of STATCOM for grid integration of wind energy systems, *IET Electric Power Applications*, vol. 12, no. 5, pp. 605–613, 2018, doi: 10.1049/iet-epa.2017.0662.
[6] Tremblay E., Atayde S., Chandra A., Comparative study of control strategies for the doubly fed induction generator in wind energy conversion systems: A DSP-based implementation approach, *IEEE Transactions on Sustainable Energy*, vol. 2, no. 3, pp. 288–299, 2011, doi: 10.1109/TSTE.2011.2113381.
[7] Abad G., Lopez J., Rodriguez M., Marroyo L., Iwanski G.,

Doubly Fed Induction Machine: Modeling and Control for Wind Energy Generation, in *Wiley-IEEE Press*, 2011, p. 625.

[8] Xu Y., Li F., Adaptive PI control of STATCOM for voltage regulation, *IEEE Transactions on Power Delivery*, vol. 29, no. 3, pp. 1002–1011, 2014, doi: 10.1109/TPWRD.2013.2291576.

[9] Routray S. K., Nayak N., Rout P. K., A Robust Fuzzy Sliding Mode Control Design for Current Source Inverter based STATCOM Application, *Procedia Technology*, vol. 4, pp. 342–349, 2012, doi: 10.1016/j.protcy.2012.05.052.

[10] Ajami A. Taheri N., A Hybrid Fuzzy/LQR Based Oscillation Damping Controller Using 3-level STATCOM, *International Journal of Computer and Electrical Engineering*, vol. 3, no. 2, pp. 184–189, 2011, doi: 10.7763/ijcee.2011.v3.312.

[11] Yunhao H., Yuanyuan S., Han Z., Yang M., Sliding mode reactive power control of isolated wind-disel hybrid power system based on STATCOM, *37th Chinese Control Conference Jul. 2018, Wuhan, China*, pp. 8709–8714, 2018.

[12] Ziaeinejad S., Mehrizi-Sani A., Design tradeoffs in selection of the DC-side voltage for a D-STATCOM, *IEEE Transactions on Power Delivery*, vol. 33, no. 6, pp. 3230–3232, 2018, doi: 10.1109/TPWRD.2017.2750422.

[13] Hamoud F., Doumbia M. L., Cheriti A., Hybrid PI-Sliding Mode Control of a voltage source converter based STATCOM, *16th International Power Electronics and Motion Control Conference and Exposition, PEMC 2014*, pp. 661–666, 2014, doi: 10.1109/EPEPEMC.2014.6980571.

[14] Routray S. K., Nayak N., Rout P. K., A Robust Fuzzy Sliding Mode Control Design for Current Source Inverter based STATCOM Application, *Procedia Technology*, vol. 4, pp. 342–349, 2012, doi: 10.1016/j.protcy.2012.05.052.

[15] Shahnia F., Rajakaruna S., Ghosh A., Static Compensators (STATCOMs) in Power Systems, in *Power Systems*, 2015. doi: 10.1007/978-981-287-281-4.

[16] Touil S. A., Boudjerda N., Boubakir A., El Khamlichi Drissi K., A sliding mode control and artificial neural network based MPPT for a direct grid-connected photovoltaic source, *Asian Journal of Control*, vol. 21, no. 4, pp. 1892–1905, 2019, doi: 10.1002/asjc.2007.

[17] Lalili D., Mellit A., Lourci N., Medjahed B., Berkouk E. M., Input output feedback linearization control and variable step size MPPT algorithm of a grid-connected photovoltaic inverter, *Renewable Energy*, vol. 36, no. 12, pp. 3282–3291, 2011, doi: 10.1016/j.renene.2011.04.027.

[18] Saravanan S. Ramesh Babu N., Maximum power point tracking algorithms for photovoltaic system - A review, *Renewable and Sustainable Energy Reviews*, vol. 57, pp. 192–204, 2016, doi: 10.1016/j.rser.2015.12.105.

[19] Belila H., Boudjerda N., BOUBAKIR A., BAHRI I., Improved STATCOM efficiency using a hybrid technique based on sliding mode control and proportional integral control, *Przeglad Elektrotechniczny*, vol. 96, no. 10, pp. 156–162, 2020, doi: 10.15199/48.2020.10.29.

[20] Saeedifard M., Space Vector Modulation of Multi-Level and Multi-Module Converters for High Power Applications, Thèse de doctorat, Université de Toronto, 2008.